




Cite this: *New J. Chem.*, 2024, 48, 13846

Received 24th June 2024,  
Accepted 8th July 2024

DOI: 10.1039/d4nj02884h

rsc.li/njc

# HF-addition to haloacetyl fluorides in superacidic media†

Sebastian Steiner, \* Zurwa M. Shafiq, Alexander Nitzer, Dirk Hollenwäger and Andreas J. Kornath‡

The reactions of difluoroacetyl fluoride and trifluoroacetyl fluoride were investigated in the binary superacid HF/SbF<sub>5</sub> by low-temperature NMR spectroscopy. Whereas both haloacetyl fluorides form oxonium species after the addition of HF, the protonated acyl fluorides were not observed. Protonated 1,1,2,2-tetrafluoroethanol was isolated as a solid and represents an example of a protonated  $\alpha$ -fluoroalcohol. The salt was characterized by low-temperature vibrational spectroscopy and single-crystal X-ray diffraction. [CHF<sub>2</sub>CF<sub>2</sub>OH<sub>2</sub>][SbF<sub>6</sub>] crystallizes in the triclinic space group  $P\bar{1}$  with two formula units per unit cell. Protonated perfluoroethanol is only stable in solution. The reactivity of both haloacetyl fluorides is discussed based on quantum chemical calculations at the MP2/aug-cc-pVTZ-level of theory.

## Introduction

Perfluorinated alcohols are of special interest in chemical syntheses. Due to their low nucleophilicity and high hydrogen bond donor strength, they are used as versatile applicable solvents and as precursors for the syntheses of weakly coordinating anions (WCAs).<sup>1–6</sup> As primary and secondary perfluoroalcohols are thermally unstable due to facile HF-elimination, only a limited number of isolated compounds are reported in the literature.<sup>7,8</sup> The simplest representative of this compound class, trifluoromethanol, was synthesized first by Seppelt from trifluoromethyl hypochlorite and hydrogen chloride at  $-110\text{ }^{\circ}\text{C}$ .<sup>9</sup> CF<sub>3</sub>OH is thermally unstable and decomposes rapidly to COF<sub>2</sub> and HF.<sup>10</sup> On a laboratory scale, perfluoroalcohols are synthesized by reacting either perfluorinated ketones or acyl fluorides in aHF.<sup>7</sup> By this method, heptafluorocyclobutanol was prepared by Baxter, and the first crystal structure of an  $\alpha$ -fluoroalcohol was elucidated by single-crystal X-ray diffraction.<sup>11,12</sup> In addition, perfluorinated methanol, ethanol, and n-propanol were synthesized from the respective acyl fluorides, and the temperature dependency of the HF-addition to these compounds was investigated by NMR spectroscopy.<sup>13</sup> Thus, the respective acyl fluoride is the predominant species at room temperature, but the addition of strong Lewis acids to HF enables the shift of the equilibrium to the side of the perfluorinated alcohols and the stabilization of these compounds as oxonium salts.<sup>13</sup>

In previous studies of our group, the properties of acetyl fluoride and haloacetyl fluorides were investigated in the binary superacidic systems HF/AsF<sub>5</sub> and HF/SbF<sub>5</sub>. While acetyl fluoride reacts under the formation of stable acetylium salts, the substitution of the CH<sub>3</sub> moiety for electron-withdrawing groups leads to the formation of protonated acyl fluorides, as in the case of chloroacetyl fluoride and fluoroacetyl fluoride.<sup>14</sup> When even more electron-withdrawing groups such as the CCl<sub>2</sub>H moiety were introduced, dichloroacetyl fluoride showed a different reactivity. Thus, oxonium salts were formed when the Lewis acid SbF<sub>5</sub> was applied in excess. Thereby, the COF moiety is protonated and then HF is added due to an increased electrophilicity of the carbonyl carbon.<sup>15</sup> Nevertheless, the intermediate protonated dichloroacetyl fluoride was isolated as a solid and characterized by single-crystal X-ray diffraction.<sup>15</sup> This prompted us to perform investigations on the properties of further haloacetyl fluorides with even more electron-withdrawing groups in superacidic media. It was the aim to investigate their reactivity regarding the addition of HF to their carbonyl bonds and to find out if there is a limit to isolating even more electron-deficient protonated haloacetyl fluorides. We herein report the reactions of difluoroacetyl fluoride and trifluoroacetyl fluoride in the binary superacidic systems HF/SbF<sub>5</sub> and DF/SbF<sub>5</sub>.

## Results and discussion

### Syntheses and properties

Difluoroacetyl fluoride (F<sub>2</sub>AcF) was reacted at  $-60\text{ }^{\circ}\text{C}$  in the binary superacidic system HF/SbF<sub>5</sub>. To trace the reactivity of the haloacetyl fluoride in superacidic media, NMR spectroscopy was performed at  $-60\text{ }^{\circ}\text{C}$ , whereas one equivalent of the Lewis

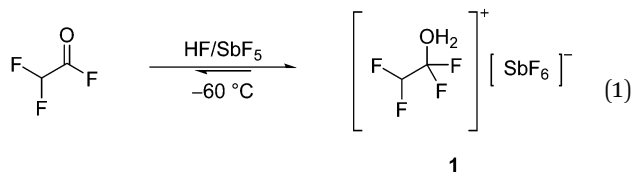
Department Chemie, Ludwig-Maximilians-Universität München, Butenandtstr. 5-13, 81377 Munich, Germany. E-mail: sebastian.steiner@cup.uni-muenchen.de

† Electronic supplementary information (ESI) available: For full details on vibrational spectroscopy, NMR spectroscopy, X-ray diffraction refinement, and computational details. CCDC 2312629. For ESI and crystallographic data in CIF or other electronic format see DOI: <https://doi.org/10.1039/d4nj02884h>

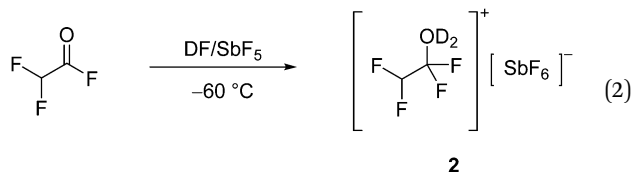
‡ Prof. Dr Andreas J. Kornath passed away in March 2024.



acid was applied. Accordingly, the measured  $^1\text{H}$ ,  $^{19}\text{F}$ , and  $^{13}\text{C}$  NMR spectra indicate the presence of  $[\text{CHF}_2\text{CF}_2\text{OH}_2][\text{SbF}_6]$  (**1**) in the solution, as presented in eqn (1). The oxonium species **1** is formed after the addition of HF to the carbonyl bond of  $\text{F}_2\text{AcF}$ .

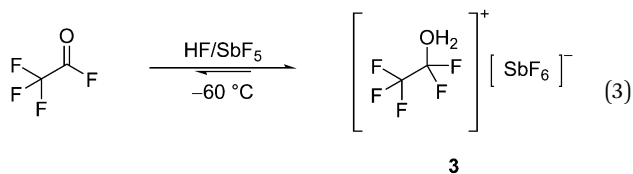


The measured NMR spectra also display an equilibrium in the solution between  $\text{F}_2\text{AcF}$  and **1**, with the oxonium species being predominant at  $-60\text{ }^\circ\text{C}$ . Protonated  $\text{F}_2\text{AcF}$  is not observed under these conditions. To isolate **1** in the solid-state phase, all volatile components were subsequently removed in a dynamic vacuum at  $-78\text{ }^\circ\text{C}$ , and  $[\text{CHF}_2\text{CF}_2\text{OH}_2][\text{SbF}_6]$  (**1**) was obtained as a colorless solid. To obtain salts of the analog D-isotopomeric species,  $\text{F}_2\text{AcF}$  was reacted at  $-60\text{ }^\circ\text{C}$  in the binary superacidic system  $\text{DF/SbF}_5$ . As presented in eqn (2),  $[\text{CHF}_2\text{CF}_2\text{OD}_2][\text{SbF}_6]$  (**2**) was obtained as a colorless solid after the removal of all volatile components at  $-78\text{ }^\circ\text{C}$ .



**1** and **2** are salts of protonated 1,1,2,2-tetrafluoroethanol and show thermal decomposition at  $-55\text{ }^\circ\text{C}$ .

To investigate the reactivity of trifluoroacetyl fluoride ( $\text{F}_3\text{AcF}$ ) in  $\text{HF/SbF}_5$ , NMR spectroscopy was performed at  $-70\text{ }^\circ\text{C}$  with one equivalent of  $\text{SbF}_5$  being applied. Analog to the observed reactivity of  $\text{F}_2\text{AcF}$  in superacidic media, the measured NMR spectra indicate the presence of  $[\text{CF}_3\text{CF}_2\text{OH}_2][\text{SbF}_6]$  (**3**) in the solution (see eqn (3)), but also the formation of an equilibrium between  $\text{F}_3\text{AcF}$  and the oxonium species **3**. As previously reported by Christe,<sup>13</sup> the equilibrium is strongly shifted to the side of **3**. Here, as in the case of  $\text{F}_2\text{AcF}$ , protonated  $\text{F}_3\text{AcF}$  is also not observed under these conditions.



Subsequently, all volatile components were removed in a dynamic vacuum at  $-78\text{ }^\circ\text{C}$ . However, the isolation of **3** as a solid was not possible and only  $\text{HF/SbF}_5$  remained in the reactor. We assume that this is due to the selected temperature of  $-78\text{ }^\circ\text{C}$ , at which the volatile components are removed in the dynamic vacuum. Since  $-78\text{ }^\circ\text{C}$  is the lowest temperature feasible for removing HF due to its melting point, the isolation of **3** from  $\text{HF/SbF}_5$  at lower temperatures is not possible. As HF and  $\text{F}_3\text{AcF}$ , which are both present in the equilibrium in the solution, are in a liquid and gaseous state, respectively, at  $-78\text{ }^\circ\text{C}$ , they are removed from the equilibrium in the dynamic vacuum. The equilibrium is then consequently shifted to the reactant side according to Le Chatelier's principle, which prevents the isolation of **3** as a solid.

### NMR spectroscopy

To trace the reactivity of difluoroacetyl fluoride and trifluoroacetyl fluoride in aHF and the binary superacidic system  $\text{HF/SbF}_5$ ,  $^1\text{H}$ ,  $^{19}\text{F}$ , and  $^{13}\text{C}$  NMR spectra were measured at  $-60\text{ }^\circ\text{C}$  and  $-70\text{ }^\circ\text{C}$ , respectively, with acetone- $d_6$  as an external standard. In Table 1, the observed NMR shifts of both starting materials, **1**, and **3** are summarized. The measured NMR spectra and the complete NMR data of  $\text{F}_2\text{AcF}$ ,  $\text{F}_3\text{AcF}$ , **1**, and **3** are listed in the ESI† (Fig. S5–S14).

The  $^1\text{H}$ ,  $^{19}\text{F}$ , and  $^{13}\text{C}$  NMR spectra of  $\text{F}_2\text{AcF}$  dissolved in aHF display an equilibrium in the solution between the acyl fluoride and the corresponding  $\alpha$ -fluoroalcohol that is formed after HF-addition. As depicted in Scheme 1, the acyl fluoride is the predominant species under these conditions as the equilibrium is strongly shifted to the side of  $\text{F}_2\text{AcF}$  (see Fig. S5 and S6, ESI†).

By first dissolving equimolar amounts of  $\text{SbF}_5$  compared to  $\text{F}_2\text{AcF}$  in HF and then adding the acyl fluoride, **1** is formed. The  $^1\text{H}$  NMR spectrum shows a triplet at 5.60 ppm, which is assigned to the  $\text{CHF}_2$  moiety, and a singlet at 9.81 ppm for the  $\text{OH}_2^+$  group. The  $^{19}\text{F}$  NMR spectrum displays a singlet at  $-90.62\text{ ppm}$  and a doublet at  $-141.33\text{ ppm}$  for the  $\text{CF}_2\text{OH}_2$  and  $\text{CHF}_2$  moieties, respectively. The NMR resonance of the  $\text{CF}_2\text{OH}_2$  moiety is consistent with values reported in the literature.<sup>13,15</sup> In the  $^{13}\text{C}$  NMR spectrum two triplets of triplets are observed at  $115.6\text{ ppm}$  and  $105.8\text{ ppm}$  for the  $\text{CF}_2\text{OH}_2$  and  $\text{CHF}_2$  moieties, respectively. Further, in the  $^{19}\text{F}$  NMR spectrum, the resonance at  $-129.19\text{ ppm}$  is assigned to the anion  $[\text{SbF}_6]^-$ .<sup>16</sup>

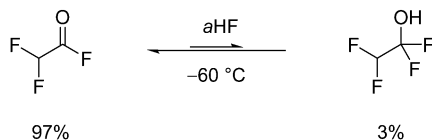
The  $^1\text{H}$ ,  $^{19}\text{F}$ , and  $^{13}\text{C}$  NMR spectra of  $\text{F}_2\text{AcF}$  dissolved in  $\text{HF/SbF}_5$  also show an equilibrium between the oxonium species **1** and  $\text{F}_2\text{AcF}$  in the solution (see Fig. S7–S9, ESI†). According to

**Table 1** Selected  $^1\text{H}$ ,  $^{19}\text{F}$ , and  $^{13}\text{C}$  NMR chemical shifts [ppm] of  $\text{F}_2\text{AcF}$ ,  $\text{F}_3\text{AcF}$ , **1**, and **3**<sup>13</sup>

	$\text{F}_2\text{AcF}^a$	<b>1</b> <sup>b</sup>	$\text{F}_3\text{AcF}^a$	<b>3</b> <sup>b 13</sup>
$\delta\text{ }^1\text{H}$ obs [ppm]	5.72 (td) ( $\text{CHF}_2$ )	9.81 (s) ( $\text{CF}_2\text{OH}_2$ ) 5.60 (t) ( $\text{CHF}_2$ )	—	9.82 (s) ( $\text{CF}_2\text{OH}_2$ )
$\delta\text{ }^{19}\text{F}$ obs [ppm]	17.74 (t) (COF) $-132.65$ (dd) ( $\text{CHF}_2$ )	$-90.62$ (s) ( $\text{CF}_2\text{OH}_2$ ) $-141.33$ (d) ( $\text{CHF}_2$ )	11.07 (q) (COF) $-78.86$ (d) ( $\text{CF}_3$ )	$-88.53$ (s) ( $\text{CF}_2\text{OH}_2$ ) $-90.97$ (s) ( $\text{CF}_3$ )
$\delta\text{ }^{13}\text{C}$ obs [ppm]	155.1 (dt) (COF) 104.7 (td) ( $\text{CHF}_2$ )	115.6 (tt) ( $\text{CF}_2\text{OH}_2$ ) 105.8 (tt) ( $\text{CHF}_2$ )	147.0 (dq) (COF) 112.6 (qd) ( $\text{CF}_3$ )	115.9 (qt) ( $\text{CF}_3$ ) 113.3 (tq) ( $\text{CF}_2\text{OH}_2$ )

<sup>a</sup> aHF as solvent. <sup>b</sup> In  $\text{HF/SbF}_5$ .





Scheme 1 Equilibrium of  $F_2AcF$  dissolved in  $aHF$  at  $-60\text{ }^\circ\text{C}$ .

Scheme 2, the equilibrium is strongly shifted to the side of the protonated  $\alpha$ -fluoroalcohol 1.

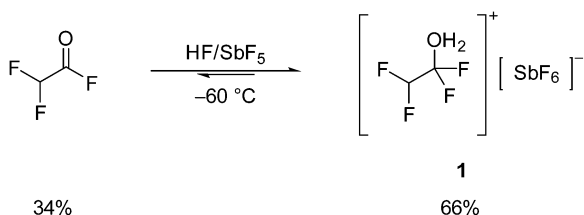
Interestingly, protonated  $F_2AcF$  is not observed under these conditions. This contrasts with the observed reactivity of dichloroacetyl fluoride ( $Cl_2AcF$ ) in the binary superacidic system  $HF/SbF_5$ . Here, an equilibrium between the analog oxonium species  $[CCl_2HCF_2OH_2][SbF_6]$  and protonated  $Cl_2AcF$  was observed in the superacidic solution at  $-60\text{ }^\circ\text{C}$ .<sup>15</sup> This is discussed in the theoretical section below.

In the case of  $F_3AcF$ , similar results to those of  $F_2AcF$  were found. The observed NMR resonances are in accordance with values previously reported by Christe.<sup>13</sup> The measured NMR spectra and the complete NMR data of  $F_3AcF$  dissolved in  $aHF$  and  $HF/SbF_5$  are listed in the ESI† (see Fig. S10–S14).

### Vibrational Spectra of $[CHF_2CF_2OH_2][SbF_6]$ (1) and $[CHF_2CF_2OD_2][SbF_6]$ (2)

The low-temperature Raman (Ra) and Infrared (IR) spectra of  $[CHF_2CF_2OX_2][SbF_6]$  (1, 2) ( $X = H, D$ ) and  $F_2AcF$  are illustrated in Fig. 1. In Table 2, selected observed Raman and IR frequencies of 1 and 2 are listed together with quantum chemically calculated frequencies of the  $HF$ -complexed cation  $[CHF_2CF_2OH_2]^+ \cdot 2HF$ , which is discussed later. The complete vibrational frequencies of 1 and 2 as well as difluoroacetyl fluoride are provided in the ESI† (Fig. S1 and Tables S1–S3).

For the  $[CHF_2CF_2OH_2]^+$  cation with  $C_1$  symmetry 24 fundamental vibrational modes are expected, all of which are Raman and IR active. The  $\nu(O-H)$  is superposed by condensed water in the IR spectra due to the measuring method. Further, the  $O-H$  stretching vibration shows low intensity in the Raman spectra due to the poor polarizability of the  $O-H$  group, which does not apply to the  $O-D$  group.<sup>17</sup> The  $O-D$  stretching vibrations of the  $D$ -isotopomeric species 2 are observed at  $2403\text{ cm}^{-1}$  and  $2286\text{ cm}^{-1}$  in the Raman spectra and at  $2403\text{ cm}^{-1}$  and  $2330\text{ cm}^{-1}$  in the IR spectra. The  $O-D$  stretching vibrations are in good agreement with values reported in the literature.<sup>14,15</sup> The  $C-F$  stretching vibrations of the  $CF_2$  moiety appear significantly blue-shifted by up to  $110\text{ cm}^{-1}$  in comparison to the neutral compound at  $1362\text{ cm}^{-1}$ ,  $1251\text{ cm}^{-1}$  (1),  $1359\text{ cm}^{-1}$ , and  $1251\text{ cm}^{-1}$  (2) (Ra) as



Scheme 2 Equilibrium of  $F_2AcF$  dissolved in  $HF/SbF_5$  at  $-60\text{ }^\circ\text{C}$ .

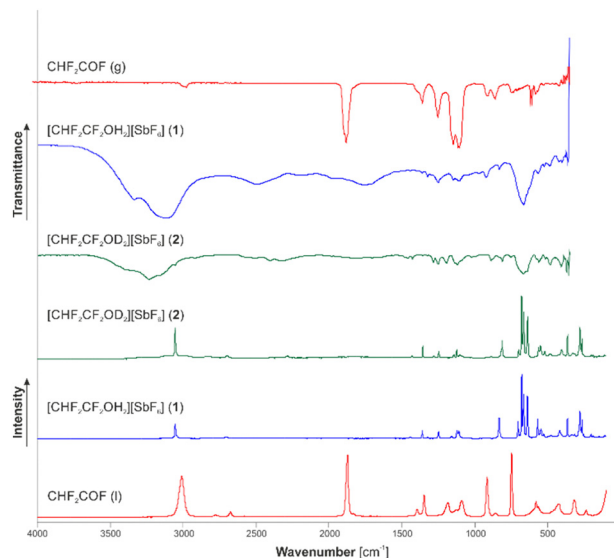


Fig. 1 Low-temperature Raman and IR spectra of  $[CHF_2CF_2OX_2][SbF_6]$  (1, 2) ( $X = H, D$ ) and vibrational spectra of  $CHF_2COF$ .

well as  $1364\text{ cm}^{-1}$ ,  $1256\text{ cm}^{-1}$  (1),  $1358\text{ cm}^{-1}$ , and  $1256\text{ cm}^{-1}$  (2) (IR).<sup>18</sup> They are in good agreement with the values reported for  $[CCl_2HCF_2OH_2][SbF_6]$ .<sup>15</sup> Further, the formation of the oxonium species is indicated by the  $C-O$  stretching vibration at  $836\text{ cm}^{-1}$  and  $816\text{ cm}^{-1}$  (2) in the Raman spectra and at  $835\text{ cm}^{-1}$  (1) and  $814\text{ cm}^{-1}$  (2) in the IR spectra. The  $\nu(C-O)$  is in accordance with values reported for protonated alcohols in the literature<sup>19,20</sup> but significantly red-shifted by approximately  $200\text{ cm}^{-1}$  compared to the  $\nu_s(C-O)$  of the analog oxonium salt  $[CCl_2HCF_2OH_2][SbF_6]$ .<sup>15</sup> The  $\nu(C-C)$  of 2 is observed at  $758\text{ cm}^{-1}$  (Ra) and  $756\text{ cm}^{-1}$  (IR) red-shifted by nearly  $100\text{ cm}^{-1}$  compared to  $F_2AcF$ .<sup>18</sup>

For the anion  $[SbF_6]^-$  with ideal octahedral symmetry more vibrations are observed than expected due to interionic interactions leading to a symmetry distortion.<sup>17</sup>

### Crystal structure of $[CHF_2CF_2OH_2][SbF_6]$ (1)

$[CHF_2CF_2OH_2][SbF_6]$  (1) crystallizes in the triclinic space group  $P\bar{1}$  with two formula units per unit cell. The molecular unit of 1 is illustrated in Fig. 2. Crystal data and structure refinement are provided in the ESI† (Table S4). Selected geometric data are listed in Table 3.

The bond length  $C1-O1$  ( $1.424(4)\text{ \AA}$ ) is significantly elongated compared to difluoroacetyl fluoride ( $1.180(5)\text{ \AA}$ )<sup>18,21</sup> and is in the range of a formal  $C-O$  single bond ( $1.432\text{ \AA}$ ).<sup>22</sup> The  $C1-O1$  bond length is consistent with the corresponding  $C-O$  bond length reported for  $[CCl_2HCF_2OH_2][SbF_6]$  ( $1.418(3)\text{ \AA}$ )<sup>15</sup> but significantly shorter than values of oxonium species or protonated alcohols reported in the literature.<sup>19,23,24</sup> The bond lengths  $C1-F1$  ( $1.318(4)\text{ \AA}$ ) and  $C1-F2$  ( $1.325(4)\text{ \AA}$ ) are slightly shortened compared to the starting material ( $1.342(7)\text{ \AA}$ )<sup>18,21</sup> and are in accordance with the  $C-F$  bond lengths of  $[CCl_2HCF_2OH_2][SbF_6]$  ( $1.325(2)\text{ \AA}$ ).<sup>15</sup> Further, the bond  $C1-C2$  ( $1.524(5)\text{ \AA}$ ) remains unchanged compared to  $F_2AcF$  ( $1.514(7)\text{ \AA}$ ).<sup>18,21</sup>

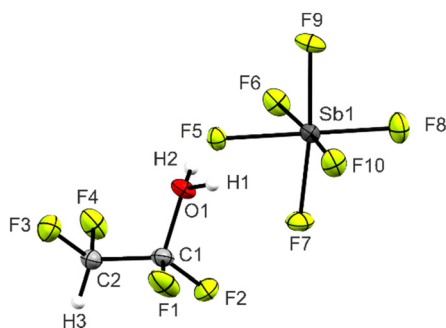
The  $Sb-F$  bond lengths of  $[SbF_6]^-$  are in the range between  $1.853(2)\text{ \AA}$  and  $1.925(2)\text{ \AA}$  and correspond with values reported



**Table 2** Selected experimental vibrational frequencies [ $\text{cm}^{-1}$ ] of  $[\text{CHF}_2\text{CF}_2\text{OH}_2][\text{SbF}_6]$  (**1**) and  $[\text{CHF}_2\text{CF}_2\text{OD}_2][\text{SbF}_6]$  (**2**) as well as calculated vibrational frequencies [ $\text{cm}^{-1}$ ] of  $[\text{CHF}_2\text{CF}_2\text{OH}_2]^+\cdot 2\text{HF}$ 

$[\text{CHF}_2\text{CF}_2\text{OH}_2][\text{SbF}_6]$ ( <b>1</b> )		$[\text{CHF}_2\text{CF}_2\text{OD}_2][\text{SbF}_6]$ ( <b>2</b> )		$[\text{CHF}_2\text{CF}_2\text{OH}_2]^+\cdot 2\text{HF}$ calc. <sup>ab</sup> (IR/Raman) <sup>c</sup>	Assignments		
Raman	IR	Raman	IR				
3055(25)		3055(50)	3053 m	2983(5/81)	$\nu_1$	A	$\nu(\text{C-H})$
1362(13)	1364 s	1359(19)	1358 w	1406(14/1)	$\nu_5$	A	$\nu(\text{C-F})$
1251(11)	1256 s	1251(12)	1256 m	1235(236/2)	$\nu_6$	A	$\nu(\text{C-F})$
1164(5)	1151 s	1144(6)		1152(181/2)	$\nu_9$	A	$\nu(\text{C-F})$
1124(13)		1125(15)	1121 m	1102(6/4)	$\nu_{10}$	A	$\nu(\text{C-F})$
836(34)	835 s	816(30)	814 m	1045(89/3)	$\nu_{12}$	A	$\nu(\text{C-O})$
		758(3)	756 w	755(67/5)	$\nu_{14}$	A	$\nu(\text{C-C})$

<sup>a</sup> Calculated at  $\omega\text{B97XD/aug-cc-pVTZ}$ -level of theory. <sup>b</sup> Frequencies are scaled with a factor of 0.956. <sup>c</sup> IR intensity in [ $\text{km mol}^{-1}$ ] and Raman intensity in [ $\text{\AA}^4 \text{u}^{-1}$ ]. Abbreviations for IR intensities: vs = very strong, s = strong, m = medium, w = weak, vs = very weak.

**Fig. 2** Molecular unit of  $[\text{CHF}_2\text{CF}_2\text{OH}_2][\text{SbF}_6]$  (**1**) (displacement ellipsoids with 50% probability).**Table 3** Selected bond lengths [ $\text{\AA}$ ] and angles [ $^\circ$ ] of  $[\text{CHF}_2\text{CF}_2\text{OH}_2][\text{SbF}_6]$  (**1**) and donor–acceptor distances. Symmetry codes: i =  $-1 + x, y, z$ ; ii =  $1 - x, -y, 2 - z$ ; iii =  $1 - x, 1 - y, 1 - z$ ; iv =  $x, 1 + y, z$ ; v =  $1 - x, 1 - y, 2 - z$ 

Bond lengths [ $\text{\AA}$ ]			
C1–C2	1.524(5)	C2–F3	1.341(4)
C1–F1	1.318(4)	C2–F4	1.346(4)
C1–F2	1.325(4)	C1–O1	1.424(4)
Bond angles [ $^\circ$ ]			
C2–C1–O1	109.1(3)	F1–C1–O1	106.3(3)
F1–C1–C2	111.9(3)	F1–C1–F2	110.0(3)
F3–C2–C1	108.1(3)	F3–C2–F4	108.5(3)
Dihedral angles [ $^\circ$ ]			
F3–C2–C1–F1	55.0(3)	F3–C2–C1–O1	−62.4(3)
F3–C2–C1–F2	178.0(2)	F4–C2–C1–F1	171.8(2)
Interatomic contacts [ $\text{\AA}$ ]			
O1(–H1)···F6i	2.471(3)	O1···F9ii	2.689(3)
O1(–H2)···F5	2.452(3)	F5···F3v	2.888(3)
C2(–H3)···F7iii	3.129(4)	F5···F9iv	2.890(2)
C2(–H3)···F10iv	3.166(4)		

in the literature.<sup>25–27</sup> Due to solid-state effects, the anion displays distorted octahedral symmetry. The bonds Sb1–F5 and Sb1–F6 are significantly longer than the other Sb–F bonds because they are involved in hydrogen bonding.

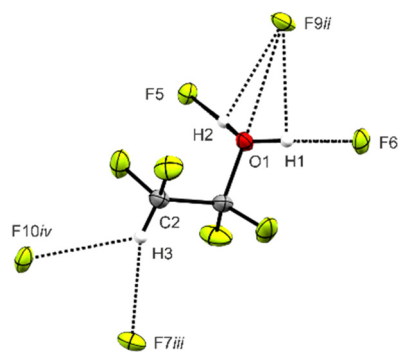
In the crystal structure of **1** the ions are arranged into chains along the *a*-axis by the strong hydrogen bonds O1(–H1)···F6i

(2.471(3)  $\text{\AA}$ ) and O1(–H2)···F5 (2.452(3)  $\text{\AA}$ ) (see Fig. 3 and Fig. S2, ESI<sup>†</sup>).<sup>28</sup> The ions also form chains along the *c*-axis by the weak hydrogen bond C2(–H3)···F7ii (3.129(4)  $\text{\AA}$ ) and the O···F interaction O1···F9iv (2.689(3)  $\text{\AA}$ ) (see Fig. 3 and Fig. S3, ESI<sup>†</sup>). Further, dimers of cation–anion pairs are formed by the intermolecular F···F contacts F5···F3v (2.888(3)  $\text{\AA}$ ) and F5···F9iv (2.890(2)  $\text{\AA}$ ) as well as the weak hydrogen bond C2(–H3)···F10iv (3.166(4)  $\text{\AA}$ ) (see Fig. S4, ESI<sup>†</sup>). All interatomic O···F and F···F contacts are below the sum of their van der Waals radii (2.99  $\text{\AA}$ , and 2.94  $\text{\AA}$ ).<sup>29</sup> Interatomic distances are listed in Table 3.

### Theoretical calculations

Quantum chemical calculations were performed at the  $\omega\text{B97XD/aug-cc-pVTZ}$ -level of theory.<sup>30</sup>  $\text{F}_2\text{AcF}$ ,  $\text{F}_3\text{AcF}$ , and  $[\text{CHF}_2\text{CF}_2\text{OH}_2]^+\cdot 2\text{HF}$  were calculated in the gas phase for a better assignment of the vibrational modes and to compare the theoretical and experimentally determined geometric parameters. Solid-state effects and intermolecular interactions were simulated by adding additional HF molecules to the cation in the gas phase.<sup>31</sup> In the ESI<sup>†</sup> (Fig. S15),  $[\text{CHF}_2\text{CF}_2\text{OH}_2]^+\cdot 2\text{HF}$  is illustrated with selected bond lengths and angles in comparison to the crystal structure. The calculated values of the HF-complexed cation are in good agreement with the experimentally obtained data.

As observed in the experimental section, the NMR spectra of  $\text{F}_2\text{AcF}$  and  $\text{F}_3\text{AcF}$  dissolved in  $\text{HF/SbF}_5$  both show equilibria between the oxonium species **1** and **3**, respectively, and their

**Fig. 3** Interionic contacts of **1** (displacement ellipsoids with 50% probability). Symmetry codes: i =  $-1 + x, y, z$ ; ii =  $1 - x, -y, 2 - z$ ; iii =  $1 - x, 1 - y, 1 - z$ ; iv =  $x, 1 + y, z$ .

corresponding haloacetyl fluorides. In both cases, the protonated haloacetyl fluorides were not observed. This is in contrast with recent studies of our group on the reactivity of dichloroacetyl fluoride in the binary superacidic system HF/SbF<sub>5</sub>.<sup>15</sup> Here, the measured NMR spectra of Cl<sub>2</sub>AcF dissolved in HF/SbF<sub>5</sub> at −60 °C displayed an equilibrium between [CCl<sub>2</sub>HCF<sub>2</sub>OH<sub>2</sub>][SbF<sub>6</sub>] and protonated Cl<sub>2</sub>AcF.<sup>15</sup> The addition of HF to the carbonyl bond of Cl<sub>2</sub>AcF was also only observed after the protonation of the C=O bond, as the carbonyl carbon displayed an increased electrophilicity due to the protonation.<sup>15</sup> To get a more detailed insight into the versatile reactivity of the haloacetyl fluorides in HF/SbF<sub>5</sub>, quantum chemical calculations were performed at the MP2/aug-cc-pVTZ-level of theory. Therefore, Cl<sub>2</sub>AcF, F<sub>2</sub>AcF, F<sub>3</sub>AcF, as well as [CCl<sub>2</sub>HC(OH)F]<sup>+</sup>·HF, [CHF<sub>2</sub>C(OH)F]<sup>+</sup>·HF, and [CF<sub>3</sub>C(OH)F]<sup>+</sup>·HF were optimized and molecular electrostatic potentials (MEPs) were calculated alongside natural population analysis charges (NPAs) (see Tables S6, S7 and S9–S13, ESI<sup>†</sup>). The calculated MEPs are shown in Fig. 4 and the calculated NPA charges are listed in Table S13 (ESI<sup>†</sup>).

As illustrated, the MEPs of the haloacetyl fluorides as well as of the protonated species show electron-deficient moieties,

so-called  $\pi$ -holes, in the region of the carbonyl carbon.<sup>14,15,32–35</sup> These indicate that electrophilic regions of the molecules are located at the carbon atoms. To quantify the influence of the electron-withdrawing substituents on the electrophilicity of Cl<sub>2</sub>AcF, F<sub>2</sub>AcF, and F<sub>3</sub>AcF as well as the protonated species, the associated MEP values at the  $\pi$ -holes of the calculated molecules are highlighted in Fig. 4. Accordingly, the most positive MEP values that were found on the MEP surfaces of the haloacetyl fluorides are 73.2 kJ mol<sup>−1</sup> (Cl<sub>2</sub>AcF), 113.9 kJ mol<sup>−1</sup> (F<sub>2</sub>AcF), and 140.8 kJ mol<sup>−1</sup> (F<sub>3</sub>AcF). Thus, the  $\pi$ -holes become significantly larger the more electron-withdrawing the adjacent substituent is. Further, the electrophilicity of the carbonyl carbon is therefore significantly increased the more electron-withdrawing the adjacent substituent is.

In the case of the protonated species, the observed MEP values at the  $\pi$ -holes are significantly higher than for the acyl fluorides.<sup>14,15,35</sup> Thus, the electrophilicity of the haloacetyl fluorides is significantly increased due to the protonation.<sup>14,15,35</sup> Interestingly, as depicted in Fig. 4, the MEP value for the  $\pi$ -hole of [CHF<sub>2</sub>C(OH)F]<sup>+</sup>·HF is significantly higher than for

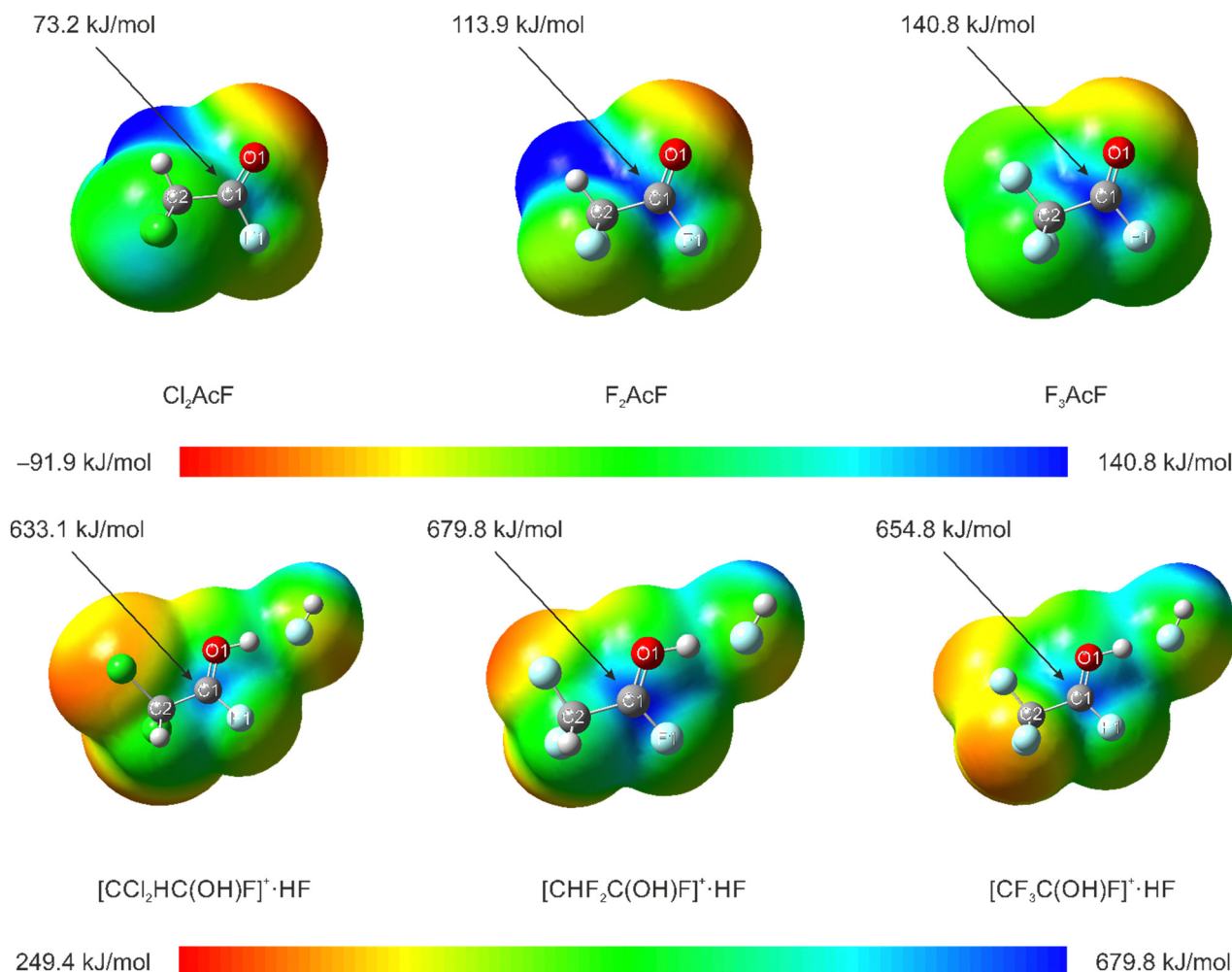


Fig. 4 Molecular 0.0004 bohr<sup>−3</sup> 3D isosurfaces with mapped electrostatic potential as a color scale from −91.9 kJ mol<sup>−1</sup> (red) to 113.9 kJ mol<sup>−1</sup> (blue) (top), and 249.4 kJ mol<sup>−1</sup> (red) to 679.8 kJ mol<sup>−1</sup> (blue) (bottom). The electrostatic potential isosurfaces have been calculated for Cl<sub>2</sub>AcF, F<sub>2</sub>AcF, F<sub>3</sub>AcF (top), [CCl<sub>2</sub>HC(OH)F]<sup>+</sup>·HF, [CHF<sub>2</sub>C(OH)F]<sup>+</sup>·HF, and [CF<sub>3</sub>C(OH)F]<sup>+</sup>·HF (bottom). Calculated at the MP2/aug-cc-pVTZ-level of theory.



$[\text{CF}_3\text{C}(\text{OH})\text{F}]^+\cdot\text{HF}$ . We assume that this is due to the stabilizing effects of  $\text{CF}_3$  moieties due to hyperconjugation and was observed before for  $\text{CF}_3$ -substituted carbocations.<sup>36</sup> In Table S13 (ESI<sup>†</sup>), the NPA charges of the calculated protonated species are listed. Accordingly, as observed before for protonated acyl fluorides, the NPA charges of the fluorine atoms that are bound to the carbonyl groups are strongly increased compared to the neutral compounds. This indicates that the positive charges located at the carbon atoms are stabilized by electron-donation of the directly bound fluorine atoms ("R-effect").<sup>14,15,32–35</sup> To further examine these trends and to quantify the influence of the electron-withdrawing substituents on the back-donation of the fluorine lone-pair electrons, NBO analyses were performed at the MP2/aug-cc-pVTZ-level of theory for  $\text{Cl}_2\text{AcF}$ ,  $\text{F}_2\text{AcF}$ ,  $\text{F}_3\text{AcF}$ , and all protonated species. Thus, for all calculated molecules strong interactions between the  $\pi^*(\text{C}=\text{O})$  and the in-plane fluorine lone-pairs were found.<sup>14,15,35</sup> The stabilization energies of these interactions, according to the second-order perturbation theory analyses, are summarized in Table 4.

As expected, the stabilization energies are significantly higher in the case of the protonated acyl fluorides compared to the neutral compounds due to the increased back-donation of fluorine lone-pair electrons.<sup>14,15,35</sup> Furthermore, for both the acyl fluorides and the protonated species, the stabilization energies of the  $n(\text{F}) \rightarrow \pi^*(\text{C}=\text{O})$  interactions increase the more electron-withdrawing the adjacent substituents become. Only in the case of  $\text{F}_2\text{AcF}$  and  $\text{F}_3\text{AcF}$ , approximately the same stabilization energies were found, which is probably again due to the hyperconjugation of the  $\text{CF}_3$  moiety.<sup>36</sup> Thus, these trends also suggest that the  $\pi$ -holes and therefore the electrophilicities of the  $\text{C}=\text{O}$  moieties increase as the neighboring substituents become more electron-withdrawing.

We therefore consequently assume that the reactivity of  $\text{Cl}_2\text{AcF}$ ,  $\text{F}_2\text{AcF}$ , and  $\text{F}_3\text{AcF}$  dissolved in  $\text{HF}/\text{SbF}_5$  is directly correlated to the electrophilicity of their carbonyl carbons. As illustrated in Fig. 4, the substitution of the  $\text{CCl}_2\text{H}$  moiety for the  $\text{CHF}_2$  and  $\text{CF}_3$  moieties leads to a significantly increased electrophilicity of the neutral compounds as well as the protonated species. This results in the favoring of the HF-addition to the carbonyl bond and consequently the shift of the observed equilibria in  $\text{HF}/\text{SbF}_5$  to the side of the protonated oxonium species. Since the  $\pi$ -hole in the case of protonated  $\text{Cl}_2\text{AcF}$  is significantly lower than in the cases of protonated  $\text{F}_2\text{AcF}$  or  $\text{F}_3\text{AcF}$ , the addition of HF to the  $\text{C}=\text{O}$  bond is less favored and

proceeds much slower. This enables the observation of the protonated intermediate in the solution and even the isolation of the species as a solid.<sup>15</sup> In the cases of protonated  $\text{F}_2\text{AcF}$  and  $\text{F}_3\text{AcF}$ , the significantly increased electrophilicity of the species leads to a more favored and faster HF-addition to the carbonyl bonds. Therefore, the protonated haloacyl fluorides were not observed in the solutions even at low temperatures. Accordingly, the substitution of the  $\text{CCl}_2\text{H}$  moiety for the  $\text{CHF}_2$  moiety represents the limit that allows the isolation of electron-deficient protonated haloacetyl fluorides from the binary superacidic system  $\text{HF}/\text{SbF}_5$ .

In addition to the calculations relating to the HF-addition, quantum chemical calculations were performed to evaluate the stability of the oxonium species **1**. As observed in the crystallographic section, the solid-state phase of **1** is strongly influenced by  $\text{O}(\text{H})\cdots\text{F}$  and  $\text{C}(\text{H})\cdots\text{F}$  hydrogen bonds. Interestingly, the optimization of the free cation  $[\text{CHF}_2\text{CF}_2\text{OH}_2]^+$  in the gas phase as an energetic minimum was only possible with a strongly extended C–O bond length compared to the crystal structure of **1**. Only the addition of HF molecules to the cation in the gas phase to simulate the strong hydrogen bonds enabled the optimization with an appropriate C–O bond length. This indicates that the intermolecular contacts have a significant influence on the bond lengths of the cation of **1** as well as on the stabilization of the compound in the solid-state phase. To further investigate this, a Hirshfeld surface analysis<sup>37,38</sup> of the intermolecular contacts was performed for the cation of **1**. In Fig. 5, the mapped Hirshfeld surface with  $d_{\text{norm}}$  of the  $[\text{CHF}_2\text{CF}_2\text{OH}_2]^+$  cation in **1** is shown, whereas the strong hydrogen bonds  $\text{O1}(\text{H1})\cdots\text{F6i}$  (2.471(3) Å)

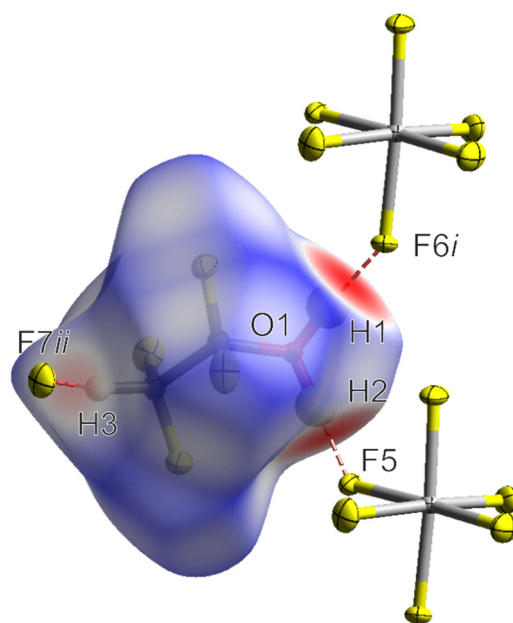


**Fig. 5** Interatomic contacts and Hirshfeld surface of the  $[\text{CHF}_2\text{CF}_2\text{OH}_2]^+$  cation in **1** (mapped with  $d_{\text{norm}}$ ).<sup>37,38</sup> Color coding of the Hirshfeld surface: white (distance  $d$  equals VDW), blue ( $d$  exceeds VDW distance), and red ( $d$  is smaller than VDW distance). For the hydrogen bond  $\text{C2}(\text{H3})\cdots\text{F7ii}$ , only the contacting fluorine atom is shown for a better visualization. Symmetry codes: i =  $-1 + x, y, z$ ; ii =  $1 - x, 1 - y, 1 - z$ .

**Table 4** Selected energies of  $n(\text{F}) \rightarrow \pi^*(\text{C}=\text{O})$  interactions from second-order perturbation theory analyses of  $\text{Cl}_2\text{AcF}$ ,  $\text{F}_2\text{AcF}$ ,  $\text{F}_3\text{AcF}$ ,  $[\text{CCl}_2\text{HC}(\text{OH})\text{F}]^+\cdot\text{HF}$ ,  $[\text{CHF}_2\text{C}(\text{OH})\text{F}]^+\cdot\text{HF}$ , and  $[\text{CF}_3\text{C}(\text{OH})\text{F}]^+\cdot\text{HF}$

Haloacetyl fluoride	Stabilization energy <sup>a</sup> [kJ mol <sup>-1</sup> ]
$\text{Cl}_2\text{AcF}$	167.7
$\text{F}_2\text{AcF}$	173.0
$\text{F}_3\text{AcF}$	172.0
$[\text{CCl}_2\text{HC}(\text{OH})\text{F}]^+\cdot\text{HF}$	270.4
$[\text{CHF}_2\text{C}(\text{OH})\text{F}]^+\cdot\text{HF}$	283.7
$[\text{CF}_3\text{C}(\text{OH})\text{F}]^+\cdot\text{HF}$	296.4

<sup>a</sup> Calculated at the MP2/aug-cc-pVTZ-level of theory.



and O(H)···F5 (2.452(3) Å) as well as the weak hydrogen bond C2(H3)···F7ii (3.129(4) Å) are highlighted. The 2D fingerprint plots of the intermolecular contacts are depicted in the ESI† (see Fig. S18).

As illustrated, the O(H)···F and C(H)···F hydrogen bonds are the predominant intermolecular contacts in the coordination sphere of the cation in **1**, with their distances being below the sum of their van der Waals radii (2.99 Å, 3.17 Å).<sup>29</sup> This is confirmed by the 2D fingerprint plots of the intermolecular contacts (see Fig. S18, ESI†). Thus, although the F···F contacts occur more often in the coordination sphere of the cation in **1** in terms of area, they have a significantly smaller influence on the structure and stability of the cation, due to their distances being equal or exceeding the van der Waals radii (2.94 Å).<sup>29</sup> The H···F contacts occur less than the F···F contacts in terms of area, but are stronger and thus more relevant for the crystal structure of **1**.

## Conclusions

The reactivity of difluoroacetyl fluoride and trifluoroacetyl fluoride was investigated in aHF and the binary superacidic system HF/SbF<sub>5</sub>. As indicated by low-temperature NMR spectroscopy, the haloacetyl fluorides form equilibria with their corresponding  $\alpha$ -fluoroalcohols in aHF. While the acyl fluorides are the predominant species in aHF at low temperatures, the addition of the strong Lewis acid SbF<sub>5</sub> enables the shift of the equilibria to the side of the  $\alpha$ -fluoroalcohols and the stabilization of these compounds as oxonium salts. Protonated 1,1,2,2-tetrafluoroethanol was isolated as a solid and characterized by low-temperature vibrational spectroscopy as well as single-crystal X-ray diffraction. Protonated perfluoroethanol is only stable in solution. Quantum chemical calculations reveal that the substitution of the CCl<sub>2</sub>H moiety for the CHF<sub>2</sub> and CF<sub>3</sub> moieties leads to a significant increase in the electrophilicity of the protonated acyl fluorides and represents the limit that allows the isolation of electron-deficient protonated acyl fluorides from HF/SbF<sub>5</sub>. The O(H)···F and C(H)···F hydrogen bonds have a significant influence on the structure and stability of protonated tetrafluoroethanol, as demonstrated by Hirshfeld surface analysis of the intermolecular contacts.

## Data availability

The data supporting this article have been included as part of the ESI†. For full details on vibrational spectroscopy, NMR spectroscopy, X-ray diffraction refinement, and computational details. Crystallographic data for [CHF<sub>2</sub>CF<sub>2</sub>OH<sub>2</sub>][SbF<sub>6</sub>] has been deposited at the CCDC under CCDC 2312629† and can be obtained from <https://www.ccdc.cam.ac.uk>.

## Conflicts of interest

There are no conflicts to declare.

## Acknowledgements

We are grateful to the Department of Chemistry of the Ludwig Maximilian University, the Deutsche Forschungsgemeinschaft (DFG), and F-Select GmbH for the financial support of this work. Special thanks go to Prof. Dr Konstantin Karaghiosoff for the help with this work after Prof. Dr Andreas J. Kornath passed away.

## References

- 1 T. W. Bentley and P. V. R. Schleyer, *Adv. Phys. Org. Chem.*, 1977, **14**, 1.
- 2 W. J. Middleton and R. V. Lindsey, *J. Am. Chem. Soc.*, 1964, **86**, 4948.
- 3 I. Krossing, *Chem. – Eur. J.*, 2001, **7**, 490.
- 4 T. J. Barbarich, S. T. Handy, S. M. Miller, O. P. Anderson, P. A. Grieco and S. H. Strauss, *Organometallics*, 1996, **15**, 3776.
- 5 J. J. Rockwell, G. M. Kloster, W. J. DuBay, P. A. Grieco, D. F. Shriver and S. H. Strauss, *Inorg. Chim. Acta*, 1997, **263**, 195.
- 6 U. P. Preiss, G. Steinfeld, H. Scherer, A. M. T. Erle, B. Benkmil, A. Kraft and I. Krossing, *Z. Anorg. Allg. Chem.*, 2013, **639**, 714.
- 7 W. A. Sheppard and C. M. Sharts, *Organic Fluorine Chemistry*, W. A. Benjamin, Inc., New York, 1969.
- 8 M. T. Nguyen, M. H. Matus, V. T. Ngan, R. Haiges, K. O. Christe and D. A. Dixon, *J. Phys. Chem. A*, 2008, **112**, 1298.
- 9 K. Seppelt, *Angew. Chem., Int. Ed. Engl.*, 1977, **16**, 322.
- 10 K. O. Christe, J. Hegge, B. Hoge and R. Haiges, *Angew. Chem., Int. Ed.*, 2007, **46**, 6155.
- 11 S. Andreades and D. C. England, *J. Am. Chem. Soc.*, 1961, **83**, 4670.
- 12 A. F. Baxter, J. Schaab, K. O. Christe and R. Haiges, *Angew. Chem., Int. Ed.*, 2018, **57**, 8174.
- 13 A. F. Baxter, J. Schaab, J. Hegge, T. Saal, M. Vasiliev, D. A. Dixon, R. Haiges and K. O. Christe, *Chem. – Eur. J.*, 2018, **24**, 16737.
- 14 S. Steiner, C. Jessen and A. J. Kornath, *Z. Anorg. Allg. Chem.*, 2022, **648**, e202200060.
- 15 S. Steiner, A. Nitzer, C. Jessen and A. J. Kornath, *Z. Anorg. Allg. Chem.*, 2024, **650**, e202400013.
- 16 P. A. W. Dean and R. J. Gillespie, *J. Am. Chem. Soc.*, 1969, **91**(26), 7260.
- 17 J. Weidlein, U. Müller and K. Dehnicke, *Schwingungsspektroskopie. Eine Einführung*, Thieme, Stuttgart, 1988.
- 18 J. R. Durig, G. A. Guirgis and T. A. Mohamed, *J. Mol. Struct.*, 1998, **444**, 165.
- 19 R. Minkwitz and S. Reinemann, *Z. Anorg. Allg. Chem.*, 1999, **625**, 121.
- 20 R. Minkwitz and V. Gerhard, *Z. Anorg. Allg. Chem.*, 1991, **603**, 95.
- 21 B. P. van Eijck, *J. Mol. Struct.*, 1977, **37**, 1.
- 22 F. H. Allen, O. Kennard, D. G. Watson, L. Brammer, A. G. Orpen and R. Taylor, *J. Chem. Soc., Perkin Trans. 2*, 1987, S1.



- 23 R. Minkwitz and S. Schneider, *Z. Anorg. Allg. Chem.*, 1998, **624**, 1989.
- 24 A. Karmakar, L. M. D. R. S. Martins, M. F. C. G. da Silva, S. Hazra and A. J. L. Pombeiro, *Catal. Lett.*, 2015, **145**, 2066.
- 25 R. Minkwitz, N. Hartfeld and C. Hirsch, *Z. Anorg. Allg. Chem.*, 1999, **625**, 1479.
- 26 R. Minkwitz and S. Schneider, *Angew. Chem., Int. Ed.*, 1999, **38**, 210.
- 27 R. Minkwitz, C. Hirsch and T. Berends, *Eur. J. Inorg. Chem.*, 1999, (12), 2249.
- 28 G. A. Jeffrey, *An introduction to hydrogen bonding*, Oxford University Press, New York, 1997.
- 29 A. Bondi, *J. Phys. Chem.*, 1964, **68**, 441.
- 30 M. J. Frisch, G. W. Trucks, H. B. Schlegel, G. E. Scuseria, M. A. Robb, J. R. Cheeseman, G. Scalmani, V. Barone, B. Mennucci, G. A. Petersson, H. Nakatsuji, M. Caricato, X. Li, H. P. Hratchian, A. F. Izmaylov, J. Bloino, G. Zheng, J. L. Sonnenberg, M. Hada, M. Ehara, K. Toyota, R. Fukuda, J. Hasegawa, M. Ishida, T. Nakajima, Y. Honda, O. Kitao, H. Nakai, T. Vreven, J. A. Montgomery, J. E. Peralta, F. Ogliaro, M. Bearpark, J. J. Heyd, E. Brothers, K. N. Kudin, V. N. Staroverov, R. Kobayashi, J. Normand, K. Raghavachari, A. Rendell, J. C. Burant, S. S. Iyengar, J. Tomasi, M. Cossi, N. Rega, J. M. Millam, M. Klene, J. E. Klene, J. E. Know, J. B. Cross, V. Bakken, C. Adamo, J. Jaramillo, R. Gomperts, R. E. Stratmann, O. Yazyev, A. J. Austin, R. Cammi, C. Pomelli, J. O. Ochterski, R. L. Martin, K. Morokuma, V. G. Zakrzewski, G. A. Voth, P. Salvador, J. J. Dannenberg, S. Dapprich, A. D. Daniels, O. Farkas, J. B. Foresman, J. V. Ortiz, J. Cioslowski and D. J. Fox, *Gaussian16, Revision C.01*, Gaussian Inc., Wallingford CT, 2016.
- 31 T. Soltner, N. Goetz and A. J. Kornath, *Eur. J. Inorg. Chem.*, 2011, 5429.
- 32 I. Alkorta, J. Elguero and A. Frontera, *Crystals*, 2020, **10**, 180.
- 33 G. Frenking, W. Koch and H. Schwarz, *J. Comput. Chem.*, 1986, **7**(4), 406.
- 34 G. A. Olah, G. Liang and Y. K. Mo, *J. Org. Chem.*, 1974, **39**(16), 2394.
- 35 M. Bayer, C. Kremser, C. Jessen, A. Nitzer and A. J. Kornath, *Chem. – Eur. J.*, 2022, **28**(15), e202104422.
- 36 A. J. Fernandes, A. Panossian, B. Michelet, A. Martin-Mingot, F. R. Leroux and S. Thibaudeau, *Beilstein J. Org. Chem.*, 2021, **17**, 343.
- 37 S. K. Wolff, D. J. Grimwood, J. J. McKinnon, M. J. Turner, D. Jayatilaka and M. A. Spackman, *CrystalExplorer 17.5, Revision: f4e298a*, University of Western Australia, 2017.
- 38 M. A. Spackman and D. Jayatilaka, *CrystEngComm*, 2009, **11**, 19.

